Type Ia Supernovae and Host Galaxy Extinction

E.D. Commins

Lawrence Berkeley National Laboratory
and Physics Department, University of California
Berkeley, California 94720

July 29, 2002

Abstract

We develop simple models for extinction of Type Ia supernova light due to dust in spiral and spheroidal host galaxies. The models are based on well-known observational facts concerning dust, galaxy morphology, and star distributions. Predictions of the models are compared with supernova data at low and high red shift.

1.Introduction

Type Ia supernovae, a relatively homogeneous class of very bright objects, have recently been employed with impressive success as distance markers in cosmological investigations. Observations of scores of Sne Ia at high red-shift z (z>0.3) have been achieved by two independent groups: the Supernova Cosmology Project (Perlmutter 1999) hereafter referred to as SCP, and the High-z research team (Riess 1998). Both groups found that the Sne Ia are somewhat dimmer than would be expected according to the magnitude-redshift relation for the Einstein- deSitter model, where Ω_m=1, Ω_Λ=0. Soon thereafter, precise observations of the fluctuation spectrum of the cosmic microwave background (CMB) were carried out (de Bernardis 2000, Balbi 2000, Jaffe 2001). These yielded the constraint $\Omega_k \equiv \Omega_m + \Omega_\Lambda = 1$. When one combines the results of the supernova and CMB studies, one is led to the conclusion that $\Omega_m \cong 0.28$, $\Omega_\Lambda \cong 0.72$. These values imply that in the present epoch, "dark energy", manifested by $\Omega_\Lambda \neq 0$, is of comparable importance to dark matter plus baryonic matter in determining the course of the Hubble expansion. Moreover, these values of Ω_m and Ω_Λ imply that the Hubble expansion is accelerating.

This unanticipated and fundamental discovery obviously demands a very high standard of evidence for its acceptance. Careful investigation of systematic effects is necessary. For example, one must determine whether extinction of supernova light by intervening dust in our Galaxy, in intergalactic space, and/or in supernova host galaxies could contribute at least in part to the observed dimming as a function of red shift.

Galactic extinction has been studied for many years and is relatively well understood (Schlegel 1998, Mathis 1990). Thus, corrections to the supernova data arising from Galactic extinction can be made with relatively high confidence, and it therefore seems very unlikely that Galactic extinction could cause a serious systematic error.

On the other hand, we know very little about possible intergalactic dust. There are no incontrovertible observations confirming its existence; only upper limits on its average density exist. Aguirre (1999a, 1999b, 2000) proposed that dimming of supernova light might be caused by intergalactic dust rather than by acceleration of the Hubble expansion. He suggested that a portion of the dust created in galaxies during intense periods of star formation in past epochs might have been driven out of these galaxies, possibly by radiation pressure. The grains with the largest opacities would be most susceptible to this pressure: these would be the long needle-like grains that have absorption coefficients relatively independent of wavelength ("gray" opacity). Such large grains would also be least susceptible to destruction by various mechanisms such as sputtering by ionized gas.

The data on one Ia supernova (1997ff) at z=1.7 appear to contradict the gray dust hypothesis and to be consistent with cosmic acceleration (Riess 2001). However the uncertainties here are quite large; also one cannot rule out the possibility that gravitational lensing is responsible for the anomalously large brightness of 1997ff (Mortsell 2001). A constraint on intergalactic gray dust can be obtained from comparison between the diffuse far infra-red background and that due to faint discrete sources (Aguirre 2000), but the uncertainties here are also too large to rule out the gray dust hypothesis categorically. A possible constraint on gray intergalactic dust may also be

forthcoming from the study of X-ray halos of distant quasars (Helfand 2002). At present, however, the best way to test the gray dust hypothesis seems to be precise measurement of the apparent magnitudes of many Sne Ia in the red-shift range $1 < z < 1.7$. Such observations could be achieved with the proposed space observatory SNAP (Linder 2001).

In this paper we concentrate on the problem of host galaxy dust. Our goal is to construct models of such dust simple enough to use and understand, but sophisticated enough to take into account the most important relevant observational facts concerning Sne Ia and their host galaxies. Work along these lines has already been done by Hatano, Branch, and Deaton (Hatano, 1998); here we try to extend their efforts. In Sec.2, we summarize the relevant observational facts underlying the models, in Sec.3 we describe the models, and in Sec.4 we compare them with additional observations. Our conclusions are presented in Sec.5.

2. The underlying observational facts.

2.1 Properties of dust.

Galactic dust is mainly confined to the Galactic plane, and its total mass is roughly 1% of the mass of interstellar gas. It consists of sub-micron sized particles, mainly graphite (and/or other forms of carbon such as nanotubes, bucky-balls, etc.), silicates, polycyclic aromatic hydrocarbons (PAHs), and some ices (NH_3, H_2O). Dust plays an important role in the energy balance of the Galaxy because it absorbs starlight (mainly in the UV and visible) and re-radiates it in the far infra-red (FIR). Perhaps 30% of the total luminosity of the Galaxy is due to this re-radiation. The opacity of dust is generally a decreasing function of wavelength; thus dust causes reddening of transmitted starlight.

Dust grains are probably formed in the outer envelopes of red giant stars and/or horizontal branch stars, as these stars suffer mass loss (Willson 2000); dust is also formed in supernova explosions. A typical grain is exposed to many physical processes and undergoes radical transformations during its lifetime [Salpeter 1977]. Grain-grain collisions can cause grains to be shattered, but in such collisions, grains can also stick together to form larger objects. Intense stellar radiation can evaporate volatile molecules from grain surfaces. UV can photo-ionize grains. Collisions with fast ions can sputter the grains (drive atoms from the grain surface). Shock waves from supernova remnants can fragment grains, and radiation pressure as well as gas-grain collisions can accelerate them. If grains are electrically charged, and a fraction undoubtedly are, then their motion is influenced by Galactic magnetic fields. All in all, a typical grain is influenced by many forces, and has a very complex history.

The absorption and reddening, which vary from one line of sight to another, are characterized by the following quantities, defined separately for each species of dust grain (as categorized by composition, size, and shape:

a) The opacity per gram of the ith component $\kappa_i(\lambda)$ in cm^2/g

b) The mass density of the i'th dust component: ρ_i in g/cm^3

From these quantities we construct the total absorption coefficient:

$$\alpha(\lambda,\mathbf{r}) = \sum_{\mathbf{i}} \rho_{\mathbf{i}}(\mathbf{r})\kappa_{\mathbf{i}}(\lambda,\mathbf{r}) \qquad \text{in cm}^{-1} \tag{1}$$

The optical depth at wavelength λ from an observer at the origin to a distance R is:

$$\tau(\lambda) = \int_0^R \alpha(\lambda,\mathbf{r})dr \text{ (dimensionless)} \tag{2}$$

The extinction, in magnitudes, is defined as:

$$A(\lambda) = 2.5 \bullet \log_{10}(e)\, \tau(\lambda) = 1.086\ \tau(\lambda) \tag{3}$$

The following quantities also appear frequently in discussions about dust:

$$E(\lambda_1 - \lambda_2) = A(\lambda_1) - A(\lambda_2) \tag{4}$$

$$R_V = \frac{A_V}{E(B-V)} \tag{5}$$

In Fig. 1 we plot $A(\lambda)/A(V)$ versus $x = \lambda^{-1}$ for 4 different values of R_V. The curves are drawn from analytical fits to large amounts of Galactic data, constructed by Cardelli, Clayton and Mathis (Cardelli 1989). These fits are represented by the equation:

$$\frac{A_\lambda}{A_{\mathbf{V}}} = a(x) + \frac{1}{R_V} b(x) \tag{6}$$

where a(x), b(x) are two purely formal analytic functions with no direct physical significance.

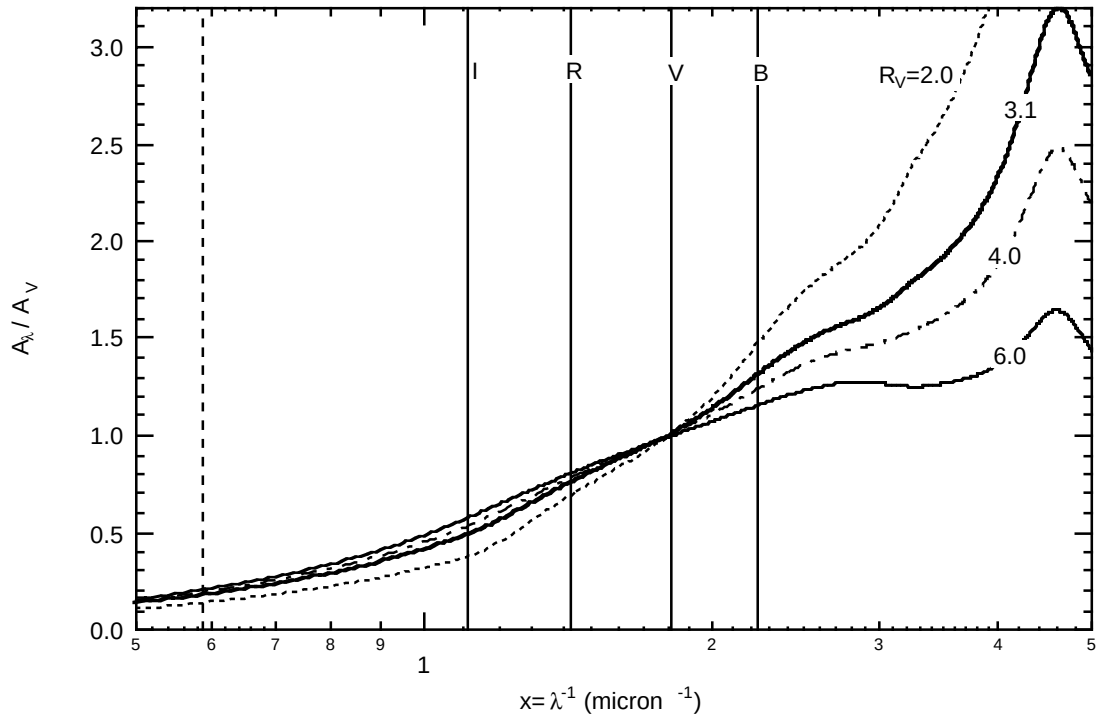

Fig.1 A_λ/A_V is plotted versus $x=\lambda^{-1}$ for 4 different values of R_V. The solid vertical lines indicate the nominal wavelengths of the standard photometric bands B,V, R, and I. The dashed vertical line corresponds to λ=1.7 microns, the planned long-wavelength-limit of observation for the proposed space observatory SNAP.

We note the following important points relevant to Fig.1.The value of R_V depends on the environment along the line of sight**.** A direction through low densities of the interstellar medium *usually* yields a low value: $R_V \approx 2$, while lines of sight through dense clouds usually give $R_V \approx 4$ to 6. A typical value for many observations in the Galaxy is R_V=3.1. For low values of R_V, $A(\lambda) / A(V)$ varies strongly with x in the UV, while for larger values of R_V, the dependence of $A(\lambda) / A(V)$ on x in the UV is much weaker. This is almost certainly due to the fact that in the interior of dense clouds, which are relatively well shielded from intense UV, various grain destruction mechanisms are diminished, and the growth of relatively large grains by coagulation is facilitated. Large grains have opacities that vary more slowly with x than small grains: this is a direct consequence of the theory of Mie scattering. In the visible and especially in the IR, the dependence of $A(\lambda) / A(V)$ on R_V is not nearly as dramatic as in the UV, as can be seen by inspection of Fig. 1 in the range $x < 2.5\ \mu^{-1}$.

The large bump in each curve of Fig.1 at $x=4.6\ \mu^{-1}$ (λ=217 nm) is probably due to graphite (and/or other stable forms of solid carbon that are spectroscopically similar). Laboratory experiments show a resonance in graphite at this wavelength with the required oscillator strength and line-width [Will, 1999]. Although it is not possible to see them in Fig.1, there are other significant resonances in the extinction curve. For example, in the visible approximately 40 absorption bands exist, the strongest of which is at 443 nm. There are also strong emission bands in the NIR at 3.3, 6.2, 7.7, 8.6, and 11.3 μ. These wavelengths all correspond to C-H or C-C bond vibrations in aromatic hydrocarbons, which could occur as polycyclic aromatic hydrocarbons and/or as more complex aromatics. Bands at 9.7 and 18 μ are probably due to SiO_4 tetrahedra in more complex structures such as olivine: $(Mg, Fe)_2\ SiO_4$. A band at 3.1μ is probably water ice or ammonia ice.

Roughly speaking, for a typical line of sight in our neighborhood of the Galaxy in B band (445 nm), $\alpha_B \approx 3\ kpc^{-1}$, corresponding to an opacity $\kappa \approx 3 \bullet 10^4\ cm^2\ g^{-1}$.

Although there is no unique prescription for the grain size distributions and for the proportions of graphite, silicates, aromatic hydrocarbons, and ices that account for all the observations, there is general agreement on a "standard Galactic dust model", first formulated by Mathis, Rumple, and Nordsieck (Mathis, 1977), developed by Draine and Lee (Draine 1984), and refined in some details by Weingartner and Draine (Weingartner 2001). According to Draine and Lee, along a "typical" line of sight, both graphite and silicate grains are distributed in size according to the formula:

$$dn_{grain} = C\ n_H\ a^{-3.5}\ da \qquad (7)$$

where a is the grain radius (for simplicity the grains are assumed to be spherical); C is a constant:

$$C_{graphite}=10^{-25.13}\ cm^{2.5} \qquad C_{silicate}=10^{-25.11}\ cm^{2.5}$$

n_H is the number density of hydrogen nuclei (in atoms or molecules), and $a_{min} \approx 50$ Angstroms, $a_{max} \approx 0.25\ \mu$. This yields a dust mass density $\approx 10^{-25}\ n_H\ g\ cm^{-3}$. Clearly the "standard" model assumes that the dust density is everywhere proportional to the

hydrogen nuclear density, it ignores the spatial variations in size and composition that are well known to occur, and it also ignores the fact that many grains are not spherical, but rather elongated "needles" with large aspect ratios. The evidence for this is the well-known phenomenon of starlight polarization, probably caused at least in part by the alignment of elongated paramagnetic grains with the Galactic magnetic field (Hall 1949, Hiltner 1949, Davis 1951, Annestad 1973) It is also known from various laboratory experiments and theoretical analyses that crystal growth from the vapor phase is strongly favored at "screw-dislocation sites", and in this case long needle-like crystals tend to form (Frank 1949, Sears 1955, Bacon 1960, Donn 1963).

The properties of dust just briefly summarized were determined almost exclusively from observations confined to our local region of the Galaxy. How can we be confident that the dust in other galaxies also has the same properties? Quantitative evidence concerning dust distributions in other spiral galaxies is obtained from a variety of sources, including IRAS surveys (Soifer 1987), ISO surveys (Genzel 2000), CCD photometry and modelling of nearly-edge-on spirals (Knapen 1991, Jansen 1994, Mathews 2001), HST observations of spirals backlit by elliptical galaxies (Keel and White 2001) and gravitational lensing of quasar light by various galaxies (Falco 1999). The data strongly suggest that the basic physical processes governing the production and evolution of dust grains are the same as in our local region of the Galaxy, but specific environmental features, such as the relative numbers of graphite and silicate grains, may vary considerably from one locale to another. In the absence of more detailed and exact knowledge, one must characterize this variation by just three (related) parameters: the dust density and opacity, and R_V or its equivalent.

2.2 Classification of the host galaxies of Type Ia supernovae

Van den Bergh, Li, and Filippenko (van den Bergh 2002) classified the host galaxies of 148 low-z supernovae, of which 50 are Ia, 11 are Ia-pec, 19 are Ibc, 60 are II, and 8 are IIn. While the core-collapse (Ibc, II, and IIn) supernovae occurred exclusively in late type galaxies with one possible exception, the Ia and Ia-pec were found in galaxies of all morphological types. This result, in agreement with earlier findings (van den Bergh 1991), is consistent with the following picture: core collapse Sne progenitors are massive stars that evolved quickly and were thus born in regions of current star formation, i.e. the spiral arms of spiral galaxies. However, Type Ia progenitors are probably C/O white dwarfs that have reached the Chandrasekhar limit by accretion from a binary companion (Hillebrandt 2000 and references therein), and could thus have originated in a variety of stellar populations, young or old.

Ivanov, Hamuy, and Pinto (Ivanov 2000) gave the host galaxy classifications of 62 separate low-z Sne Ia previously discussed by Phillips et al (1999).

Sullivan and Ellis (Sullivan 2002) classified the host galaxies of most of the high redshift Sne Ia employed by SCP in (Perlmutter 1999), some additional SCP high-z Sne Ia, and a number of low-redshift Sne Ia previously discussed (Ivanov 2000, Phillips 1999).

In Table 1. we summarize the low –z results of van den Bergh et al, and Ivanov et al; and the high-z results of Sullivan and Ellis. The Sne Ia are distributed in 3 broad

categories of galaxies: Spheroidal (E and S0); early spirals: (Sa,Sab,Sb); and late spirals and irregulars (Sbc,…).

Table 1. Numbers of SneIa found in galaxies of various morphological types.

	Spheroidal (E/S0)	Early Spiral	Late spiral, irreg.
Ivanov et al	23	17	22
van den Bergh et al	15	34	12
Sub-total (low-z)	38	51	34
Sullivan and Ellis (high z)	10	10	19

The data of Table 1. suggest that for low-z, the frequency of Sne Ia from early spirals is slightly larger than for the other two categories; while for high-z, the frequency of Sne Ia from late spirals and irregulars dominates. This may be due at least partly to the fact that at large z (z≈1), the population of irregular galaxies (mainly blue dwarfs) relative to that of large spirals and ellipticals was considerably higher than it is today (Brinchmann 1998).

2.3 Relevant properties of spiral galaxies.

A spiral galaxy consists of a relatively thin disk and a central bulge, as well as an extended halo. Bulges are frequently not spherically symmetric, and can even be triaxial, but it is a reasonable first approximation to assume spherical symmetry. The surface brightness I(R) of the typical bulge is then reasonably well described by the deVaucouleurs distribution (deVaucouleurs 1948, Binney 1998):

$$I = I_e \exp\left\{-7.67\left[\left(\frac{R}{R_e}\right)^{1/4} - 1\right]\right\} \qquad (8)$$

where R, R_e are in plane polar coordinates, and R_e is the effective radius within which 1/2 of the surface luminosity is contained. A median value of R_e for a wide range of spirals is R_e=2.6 kpc (Kent 1985, Simien and deVaucouleurs 1986). According to Simien and deVaucouleurs there is no pronounced dependence of the median R_e on Hubble T type, except for a possible weak maximum at T=1, and a slight drop for T>6.

It can be shown that the spherically symmetric luminosity density j(r) is related to the surface brightness by the formula:

$$j(r) = -\frac{1}{\pi}\int_r^\infty \frac{\partial I}{\partial R}\frac{dR}{\sqrt{R^2 - r^2}} \qquad (9)$$

where r is in spherical polar coordinates. The simple function:

$$j_B(r) = \frac{const}{r(1+2.25r)^2}$$

with r in kpc, yields a reasonably good fit to j(r) for R_e=2.6 kpc, in the range 0<r<5 kpc. However, even the simpler function:

$$j_B(r) = \frac{\text{const}}{\text{r}^3 + a^3} \qquad (10)$$

where a=.34 kpc, is adequate for our purposes.

Can we assume that the bulge luminosity density j(r) faithfully describes the distribution of Sne 1a progenitors in the bulge? This is plausible, since the bulge consists mainly of old stars, and as we have mentioned, Type Ia progenitors appear to be C/O white dwarfs driven to the Chandrasekhar limit by accretion from binary companions.

The relative importance of bulge and disk in a spiral galaxy can be characterized by the bulge-to-total luminosity ratio B/T. One finds (see Table 2) that B/T decreases systematically as one goes from early to late spiral types

Table 2. Bulge/total luminosity ratios vs galaxy morphological type.

Hubble type	B/T
S0-S0a	.42-.85 (median=.75)
Sa-Sab	.35-.61 (" =.41)
Sb-Sbc	.13-.39 (" =.25)
Sc+	.03-.2 (" =.05)

The radial brightness distribution of disk stars in a spiral galaxy is usually characterized by the function:

$$I_D(r_0) = const \sum \exp\left(-\frac{r_0}{h}\right) \qquad (11)$$

where r_0 is in cylindrical polar coordinates; (Binney 1998). In Fig.2 we show the distribution of h found by Kent (1985) for 74 spirals, where we assume that the Hubble constant is H_0=65 km s^{-1} Mpc^{-1}. The contribution to the luminosity of an axially symmetric disk with brightness profile (11) from an annular ring between r_0 and r_0+dr_0 is proportional to $r_0 \bullet \exp(-r_0/h) \bullet dr_0$; hence the fractional luminosity from stars inside the circle of radius r_0 is:

$$P(r_0)=(1-\exp(-r_0/h))-(r_0/h)\bullet\exp(-r_0/h) \qquad (12)$$

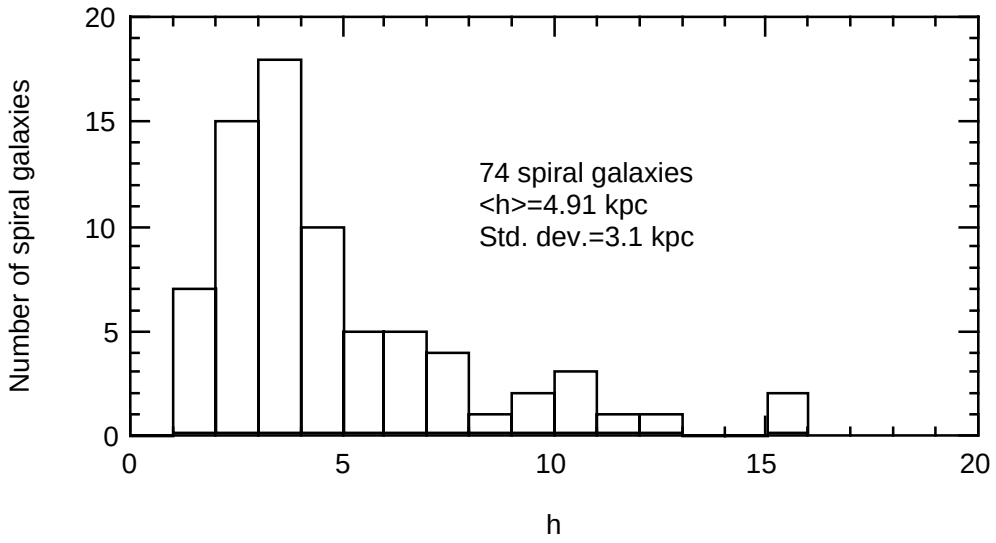

Fig.2 Distribution of disk radial scale factor h for 74 spiral galaxies (Kent 85). The following value of the Hubble constant is assumed: H_0=65 km s^{-1} Mpc^{-1}.

The "90% isophote" (where P=0.9) occurs for $r_0 \approx 4h$. Median radii for various morphological types are given in Table 3, taken from Roberts and Haynes (Roberts 1994). While it is not stated explicitly in Roberts and Haynes that these are 90 % isophotes, we shall assume this to be the case. Then, the listed values are reasonably consistent with the range of values of h shown in Fig.2 for spiral galaxies.

Table 3. Median radii of various galaxies.

Hubble type	R,kpc
E,S0	21.1
S0a,Sa	19.8
Sab,Sb	25.1
Sbc,Sc	22.4
Scd,Sd	17.7
Sm, Im	8.5

One should view the results shown in Fig. 2 and in Table 3 with care because of possible observational bias: the galaxies chosen for study by Kent, and by Roberts and Haynes, are relatively luminous, and somewhat different results might have appeared if faint galaxies had also been included. On the other hand, there is considerable evidence that the probability per unit time that a supernova will be observed in a galaxy of any given morphological type is proportional to the luminosity of that galaxy (van den Bergh 1991, Aldering 2002). Thus the host galaxies of observed supernovae are also likely to be relatively bright. In any event, as we show later, the results of our spiral galaxy model

based on (11) turn out to be very insensitive to the choice of h over a very wide range of values.

Does the disk brightness function (11) correspond to the radial distribution of disk Sne Ia progenitors? This is not evident a priori, since disks often contain young stellar populations responsible for a large fraction of the disk luminosity, whereas Sne Ia progenitors may be quite old. Nevertheless we shall assume that the two distributions are the same.

In a typical spiral galaxy, the disk stellar population z-distribution (where z is normal to the disk plane) can be modeled by the function $\mathrm{sech}^2(z/h_z)$, where $h_z \approx .33$ to .5 kpc or even 1 kpc is the scale height (Binney 1998). The scale height of observed white dwarfs (in our locale of the Galaxy) is approximately .3 kpc (Ishida 1982, Fleming 1986). Thus we shall assume that the scale height for Sne Ia is 0.33 kpc.

Although dust distributions are frequently very complicated and chaotic on a scale of 1-10 pc, regularities do commonly emerge on a sufficiently large scale (≥ 50 pc). The distribution in z can be modeled by the function $\mathrm{sech}^2(z/z_D)$, where the dust scale height z_D is typically ≈ 0.1 kpc, considerably smaller than that of the disk stars. In a spiral galaxy, dust tends to be concentrated in spiral arms, but for simplicity we can model the dust distribution in a typical disk as axially symmetric, with an exponential or Gaussian radial distribution. More details on these points are given in Sec. 3.

2.4 Relevant properties of spheroidal (E,S0) galaxies.

"Spheroidal" galaxies, like bulges in spiral galaxies, are not spherically symmetric and are frequently even triaxial, but it is a reasonable first approximation for the purpose of modeling to assume spherical symmetry. Usually, the surface brightness distribution can then be approximated by the deVaucouleurs law (eq. 8), and it is an adequate approximation to describe the underlying stellar distribution by a simple function such as:

$$\rho(r) = \rho_0 \frac{1}{1 + \frac{r^3}{c^3}} \qquad (13)$$

where ρ_0 is the central density, while the constant c sets the radial scale and is typically ≈0.1 kpc. The outer radius of the galaxy can be chosen to fix the total galaxy mass, and is typically 100 kpc.

We can obtain some idea of the dust content in spheroidal galaxies by considering the median values of far-infra-red brightness BR (in solar luminosity per pc^2), far infra-red luminosity L (in 10^9 solar luminosities), and hydrogen gas mass M (in 10^9 solar masses); all collected in Table 4. These numbers suggest that the median dust mass for E/S0 galaxies is roughly 10^6 solar masses, or ≈ 10% of that in early spirals.

Another significant clue comes from observed color gradients in elliptical galaxies. Traditionally these have been attributed to variation in stellar population with respect to radial distance from the galaxy center. However Wise and Silva (Wise 1996) suggest that dust may play an important, and perhaps dominant, role in establishing the color gradients. They have carried out a radiative transport calculation, including the effects of scattering, and find the best fit to observed color gradients in a sample of 52

elliptical galaxies by assuming a dust distribution of the form: $(r^2+d^2)^{-1/2}$ with d≈.1 to 1 kpc (spherical symmetry assumed), a large-r cutoff of 10 to 30 kpc, and the central dust density fixed to yield, once again, a total dust mass of approximately 10^6 solar masses.

Table 4. Median far-infra-red brightness BR (in solar luminosity per pc ^{2}), far-infra-red luminosity L (in 10^9 solar luminosities), and hydrogen gas mass M (in 10^9 solar masses) for galaxies of various types. Data from (Roberts 1994).

Hubble Type	BR	L	M
E,S0	3.77	1.71	1.24
S0a,Sa	11.47	9.89	5.62
Sab,Sb	9.22	14.26	15.14
Sbc,Sc	6.73	9.87	15.85
Scd,Sd	3.63	4.05	9.33
Sm, Im	7.44	1.63	2.40

3. The Models

3.1 Spiral galaxies

Fig. 3 shows the geometry used for our model of spiral galaxy host extinction. We assume an axially symmetric galaxy with origin at O. Consider a plane parallel to the galactic plane, but displaced from it by a distance z_0 (O'O=z_0). Let P be the location of the supernova in that plane, at radial distance r_0 from O'. Let PP' be a vector directed toward the observer, through a small element of dust at P'. PP' is inclined by angle θ with respect to the normal to the galactic plane. Let the projection of PP' in the plane be PQ, of length r. Construct the diameter AB through O' that is parallel to PQ. Then the plane polar coordinates ρ, z of the element of dust are given by:

$$\begin{aligned}\rho &= \sqrt{r^2 + r_0^2 - 2rr_0\cos\beta} \\ &= \sqrt{R^2\sin^2\theta + r_0^2 - 2Rr_0\sin\theta\cos\beta}\end{aligned} \tag{14}$$

and

$$z = z_0 + R\cos\theta \tag{15}$$

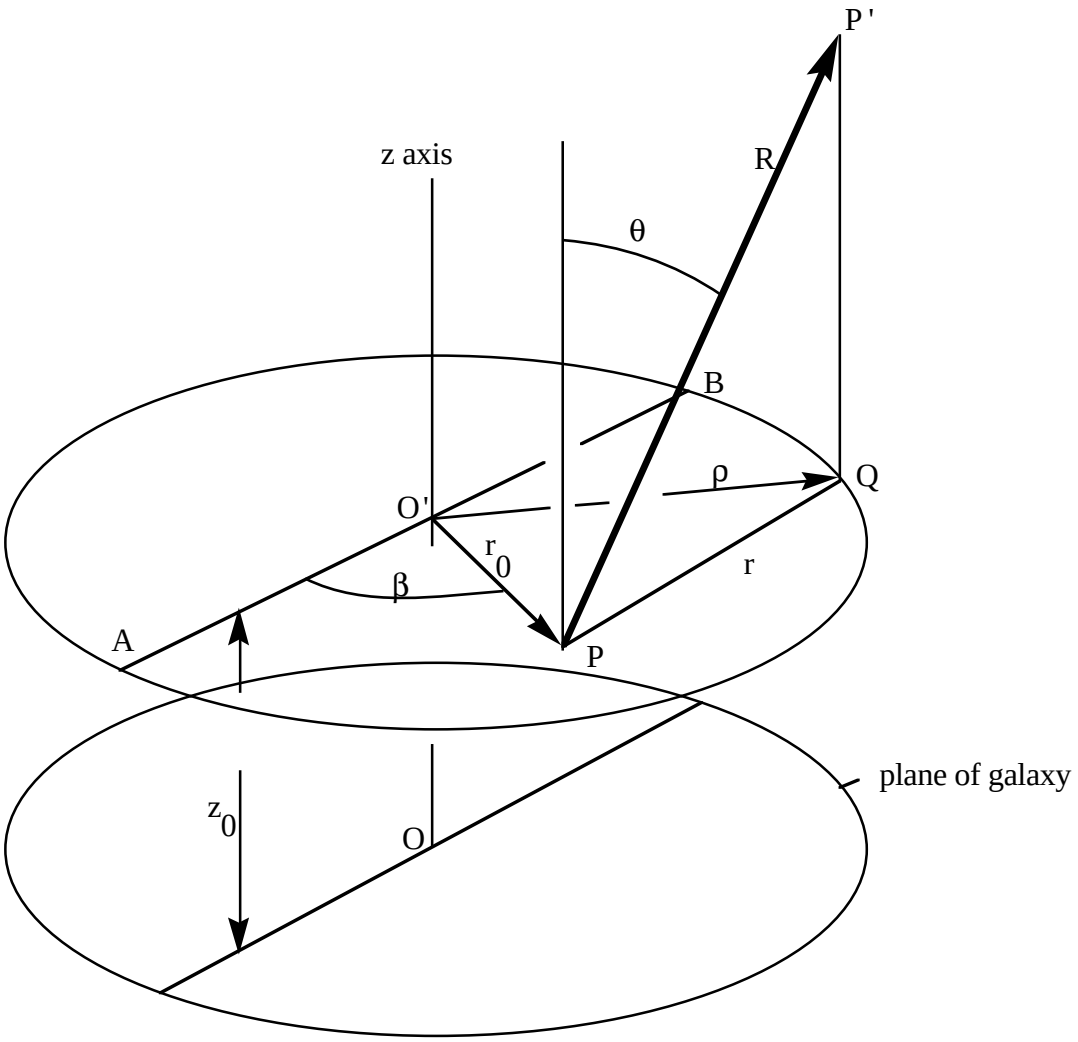

Fig.3. Geometry of spiral galaxy extinction model. Center of galaxy located at O; supernova at P; dust element at P'. Line of sight from supernova to observer is along vector **R**.

Given the location of the supernova at P= (r_0, z_0, β), the inclination angle θ, (both chosen by the Monte Carlo method) and the absorption coefficient α_B as a function of ρ, z, we use (1,14,15) to calculate the extinction:

$$A_B = 1.086\int_0^\infty \alpha_B(\rho,z)dR \qquad (20)$$

by numerical integration. We shall now describe the prescriptions for choosing P and θ , and also specify the functional form of α_B. All linear distances are in kpc.

The supernova disk distribution is:

$$f(r_0) = const \sum \exp\left(-\frac{r_0}{h}\right)\mathrm{sech}^2(3z_0) \qquad (21)$$

where in most calculations h=5 kpc; see Fig.2. Note in fact that all results are very insensitive to the choice of h, anywhere in the range $1 \le r \le 14$ kpc. . The disk supernova scale height in (21) is obviously 0.33 kpc. The supernova bulge distribution is:

$$g(r_B) = \frac{const}{r_B{}^3 + (.34)^3} \qquad (22)$$

where r_B locates the supernova in spherical polar coordinates; (see eqn (10)). The probability B/T of finding a supernova in the bulge can be chosen at will; typical values are B/T= 0, .15, .40, .75; (recall Table 2). The absorption coefficient α_B is given by the formula:

$$\alpha_B(\rho,z) = 6b \sum \exp\left[-\left(\frac{.4\rho}{h}\right)^2\right] \mathrm{sech}^2(10z) \qquad (23)$$

Here b is an important "dust density" factor that can be chosen at will. Typical values in most calculations are in the range 0.1 to 10. The Gaussian radial distribution in (23) is chosen to give a reasonable fit to IRAS observations of dust in our Galaxy for h= 3 kpc, and (23) specifies a dust scale height of .1 kpc. Also, cos θ can be held fixed or chosen randomly and uniformly between any two desired limits, such as 0 and 1.

So far we have assumed that all of the dust in a spiral galaxy originates in the disk, but one may properly ask whether the bulge might also contain dust. After all, bulges in spiral galaxies are similar to elliptical galaxies, and the latter do have dust (see Secs 2.4 and 3.2). In fact we have extended the model just described to include this possibility, but we find that the resulting changes in numerical results are relatively small, and can be neglected. Thus in what follows, we continue to assume that all of the dust in our model spiral galaxy originates from the disk.

Many of the features in the model we have described, with the exception of the quantity b, were included in somewhat simpler form in the earlier model of Hatano, Branch, and Deaton (Hatano 98).

We now illustrate several important features of the model by showing some results of calculations. In Fig. 4 we plot a histogram of the probability p(A) to find a supernova with B-band extinction between A and A+.02, as a function of A, for the following conditions: b=1, cos θ=1 (galaxy face on) and B/T=0. Also plotted is P(A), the *cumulative* probability that a supernova has extinction less than or equal to A. Two features of p(A) are typical for all our results with the spiral galaxy model. The first is the sharp peak at A≈0, which means that a large fraction of supernovae have little or no extinction. These are the supernovae on the "near side" of the galaxy: light from them encounters little or no dust on its way to the observer. The second feature is the long tail in p(A) extending to large extinctions. Obviously this is due to supernovae embedded deep within the galaxy or on the far side. The distribution p(A) is so asymmetrical that the average extinction <A> of all supernovae is not always a very useful statistic. It is often more convenient to use the median A(.5) such that P[A(.5)]=.5; and, for example, the 80th percentile: A(.8) such that P[A(.8)]=.8. For the conditions of Fig. 4, <A>=.39,

A(.5)=.19 and A(.8)=.81. Note also that since the absorption coefficient α_B is proportional to b, <A>, A(.5), and A(.8) are also proportional to b.

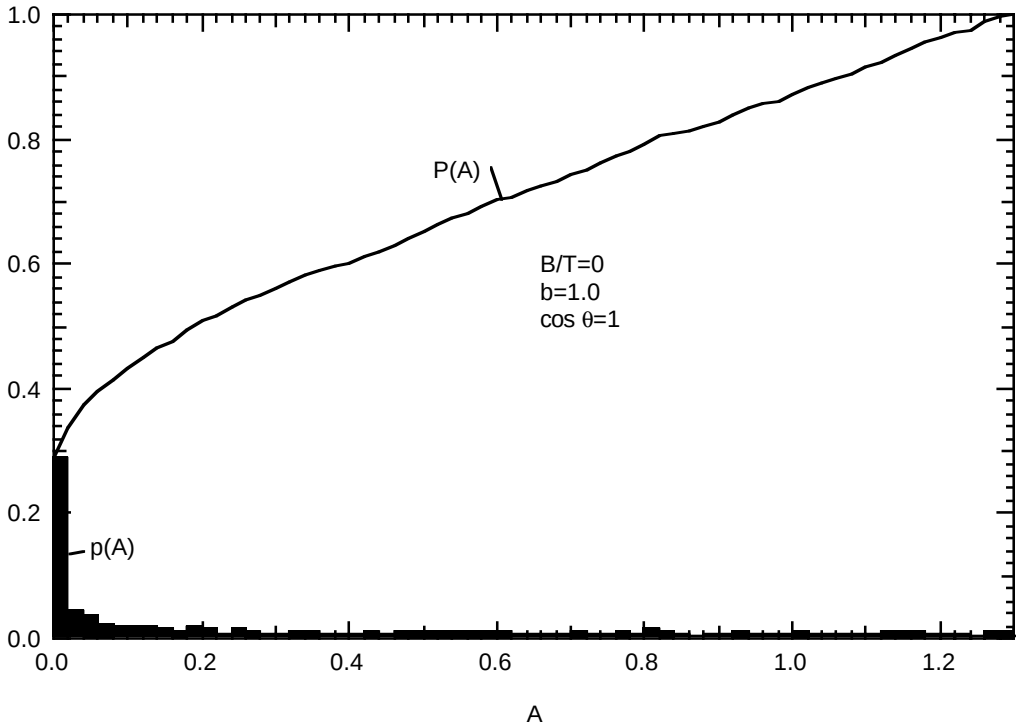

Fig. 4. The probability distribution p(A) and the cumulative probability P(A) are plotted versus B-band extinction A for the conditions b=1, cos θ=1, and B/T=0 (no supernovae in the bulge). This Monte Carlo calculation was done with 2000 supernovae.

Fig. 5 shows how A(.5) depends on the inclination angle θ, and on the relative number B/T of supernovae in the bulge, for b=1. The dependence on B/T is seen to be very weak. The dependence on θ is also weak from 0 to 40°; but then A(.5) increases rapidly for angles approaching 90° This has obvious implications for observational bias against detecting supernovae in edge-on galaxies.

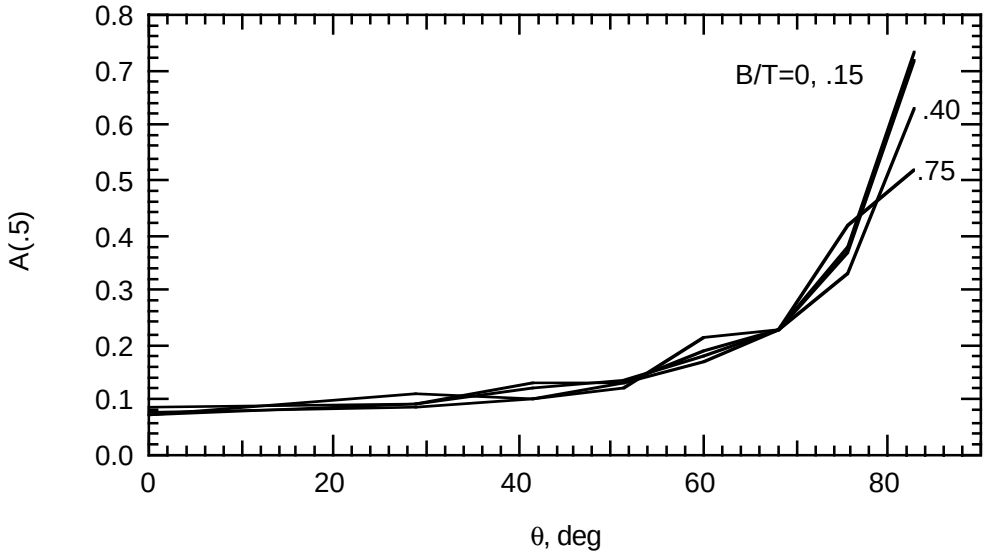

Fig. 5 A(.5) is plotted versus θ for b=1 and B/T=0, .15, .40, and .75.

In Fig. 6 we show how A(.5) and A(.8) depend on fixed values of h for B/T=.15, b=1, and cos θ uniformly and randomly chosen between 0 and 1. Clearly, A(.5) and A(.8) are virtually constant over the entire range of h. This justifies a posteriori the choice h=5 kpc that we have made for most of our calculations.

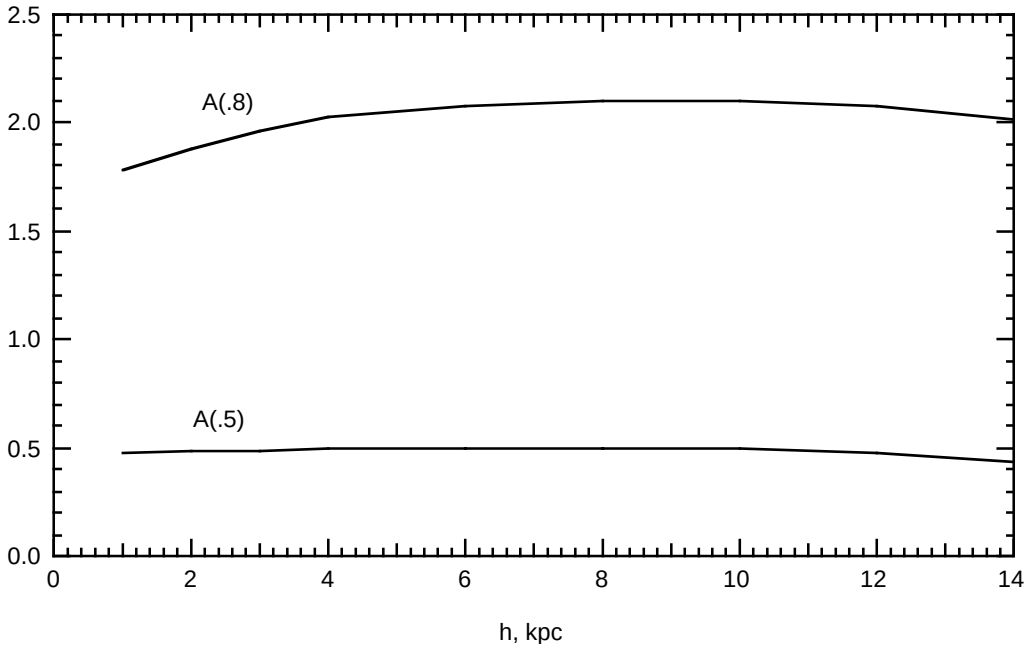

Fig. 6 A(.5) and A(.8) versus fixed h, for B/T=.15, b=1.0, and cos θ uniform and random between 0 and 1.

Fig. 7 illustrates the effect of observational selection on the detection of supernovae close to the center of a spiral galaxy. Here the white histogram shows the probability to observe a supernova in an annular ring between r_0 and r_0 + 2 kpc, vs. r_0, regardless of extinction; while the black one shows the same probability for all supernovae with extinction $A \leq 0.5$. Obviously the ratio of the "black probability" to the "white probability" decreases as one goes closer to the origin. A somewhat similar result would be obtained for calculation of the radial dependence of galactic starlight itself, except that here it would be necessary to take into account the significant effects of scattering as well as absorption, by a proper radiative transport calculation.

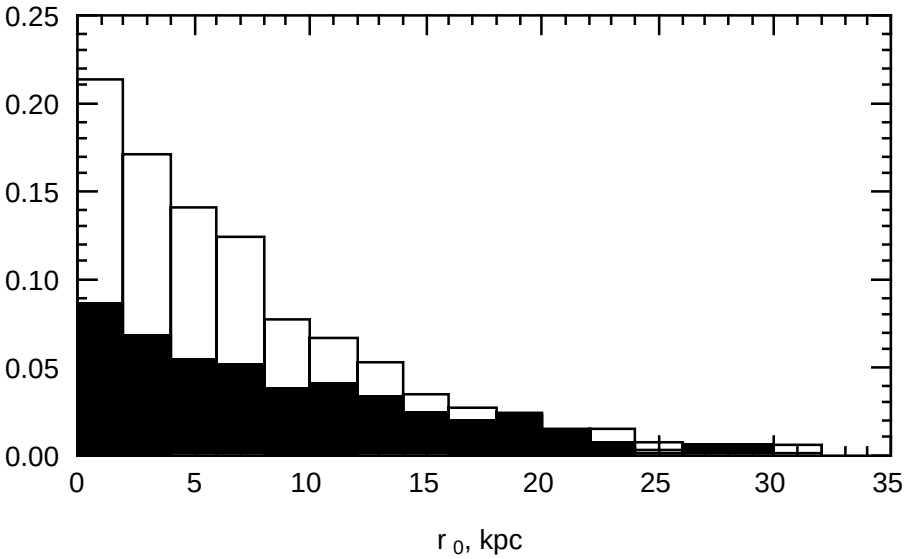

Fig. 7. White histogram: Probability to observe a supernova originating in annular ring between r_0 and r_0+2 kpc, vs. r_0, regardless of extinction. Black histogram: same probability for supernovae with extinction $A \leq 0.5$. Here, B/T=.15, b=1, and cos θ randomly and uniformly chosen between 0 and 1.

We next consider another important effect of observational selection. This arises from the fact that for any assumed values of Ω_m and $\Omega_{\Lambda,}$ the apparent magnitude m of a "standard" Type Ia supernova increases as z increases. Now, given constant conditions of observation such as telescope and detector sensitivity, seeing, etc., there is a limiting red shift $z=z_0$ corresponding to a maximum apparent magnitude m_0 beyond which one cannot observe a SN1a reliably. For the proposed space observatory SNAP, $z_0 \approx 1.7$. The observational selection effect we refer to arises because as z approaches z_0 from below, less and less extinction from host galaxy dust can be tolerated before we reach m_0.
To put this on a quantitative basis, we recall the magnitude red-shift relation, derived from Friedmann's equation (Carroll 1992). Assuming that $\Omega_m+\Omega_\Lambda = 1$ this may be written:

$$m = M + 5\log_{10}\left[(1+z)\int_0^z \frac{dx}{\sqrt{1+x\left(x^2+3x+3\right)\Omega_m}}\right] + C \qquad (24)$$

where M is the absolute magnitude of a standard SN1a and C is a constant. Now, let A_0 be the limiting extinction which at $z < z_0$ increases the magnitude m to m_0:

$$A_0 = m_0 - m \tag{25}$$

Then from (24) we obtain:

$$A_0 = 5\,log_{10}\left[\frac{(1+z_0)\int_0^{z_0}\frac{dx}{\sqrt{1+x(x^2+3x+3)\Omega_m}}}{(1+z)\int_0^{z}\frac{dx}{\sqrt{1+x(x^2+3x+3)\Omega_m}}}\right] \tag{26}$$

Numerical evaluation of (26) for z_0=1.7 reveals that to a good approximation:

$$A_0(\Omega_m = 0.3, \Omega_\Lambda = 0.7) = 2.65\ln\left(\frac{1.7}{z}\right) \tag{27}$$

and

$$A_0(\Omega_m = 1, \Omega_\Lambda = 0) = 2.32\ln\left(\frac{1.7}{z}\right) \tag{28}$$

where (27,28) are valid approximations for $z \geq 0.2$.

In Fig. 7 we plot the average extinction <A> of all supernovae with extinction less than $A_0(z)$, as a function of z, for b=.2, .4, .8, 1.6, 3.2, and 6.4. (Here we assume that Ω_m=.3, Ω_Λ=.7.) The figure reveals an important feature: as b is increased, <A> saturates over a wide range of z. In other words, as we increase b, the density of dust increases, hence more and more supernovae acquire such large extinctions that they can no longer be observed. The remaining supernovae, which can be observed, are fewer and fewer in number, but they have constant average extinction at given z for sufficiently large b. Needless to say, this saturation effect is also seen if we plot the median extinction A(.50) or the 80th percentile extinction A(.8) of all supernovae with extinction less than $A_0(z)$.

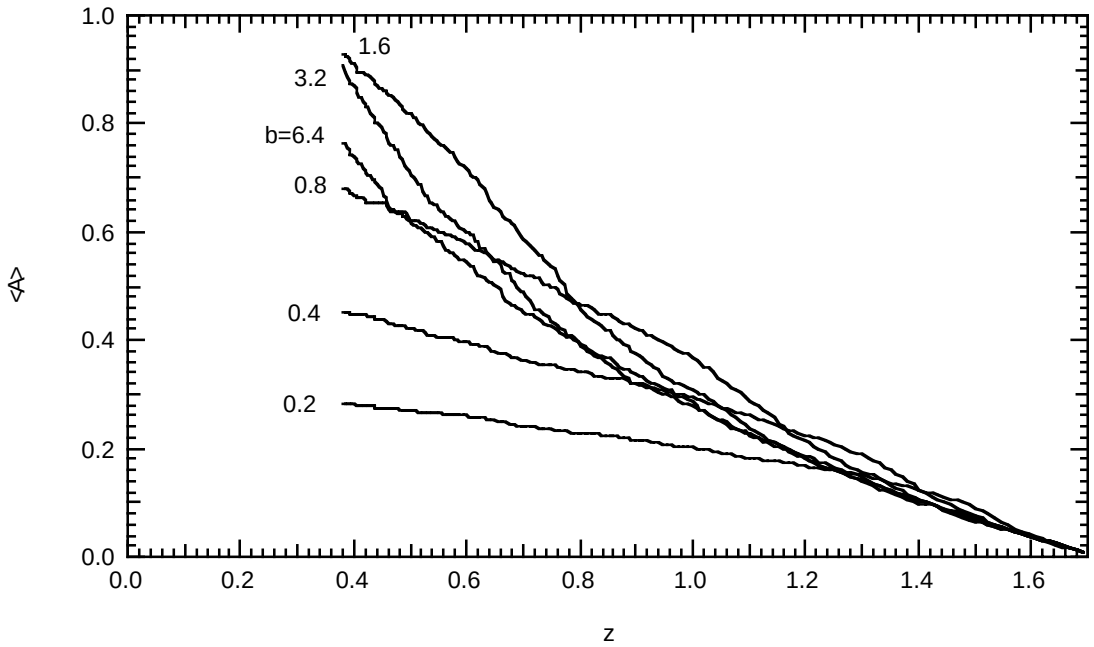

Fig. 8 Average extinction <A> of all supernovae with $A \le A_0$ plotted versus z for b=.2, .4, .8, 1.6, 3.2, 6.4; for the case z_0=1.7.

3.2 The spheroidal galaxy model

To construct a dust model for elliptical and S0 galaxies we ignore the fact that such galaxies are not usually spherically symmetric and are sometimes even triaxial: we assume spherical symmetry. Also we make use of the conclusions found by Wise and Silva (Wise 96) in their analysis of color gradients of elliptical galaxies; see Sec. 2.4. Thus we assume a supernova distribution of the form:

$$j(r) = \frac{const}{r^3 + a^3} \qquad \text{r} \le 100 \text{ kpc} \qquad (29)$$

where a=.1 kpc. The B-band dust absorption coefficient takes the form:

$$\alpha_B(r) = \frac{\kappa \rho_D}{\sqrt{1 + \left(\frac{\text{r}}{\text{r}_D}\right)^2}} \qquad (30)$$

where κ is the opacity (typically $\kappa \approx 3 \cdot 10^4$ cm^2 g^{-1}), ρ_D is the central density, and r_D can be chosen in the range 0.1 to 1 kpc. (The final results are very insensitive to r_D; hence in practice we shall simply set r_D=1 kpc.) The quantity ρ_D is fixed by the equation:

$$M_D = 4\pi\rho_D \int_0^R \frac{r^2 dr}{\left(1+\frac{r^2}{r_D^2}\right)^{1/2}}$$
$$= 2\pi\rho_D r_D^3 \left[\frac{R}{r_D}\sqrt{1+\left(\frac{R}{r_D}\right)^2} - \ln\left(\frac{R}{r_D}+\sqrt{1+\left(\frac{R}{r_D}\right)^2}\right)\right] \quad (31)$$

where M_D is the total dust mass, and R is the outer radius of the dust distribution. In our Monte Carlo model, R takes the values 5, 10, 15,20, or 30 kpc.

Fig. 8 shows the results of a Monte Carlo calculation with R=5 kpc using 5000 supernovae distributed randomly according to (29), and with $M_D=10^6$ solar masses. We plot a histogram of the probability p(A) to find a supernova with extinction between A and A+.01, versus A. As in Fig.4, we note that p(A) has a sharp peak at A≈0, but also a substantial tail extending to A > 0. In the present case, because the total dust mass is an order of magnitude less than in a spiral galaxy, and also because it is now more extended spatially, the extinction is far smaller. For the results shown in Fig.8, the 90th percentile extinction is A(.9)=.096 and the average extinction is <A>=.051.

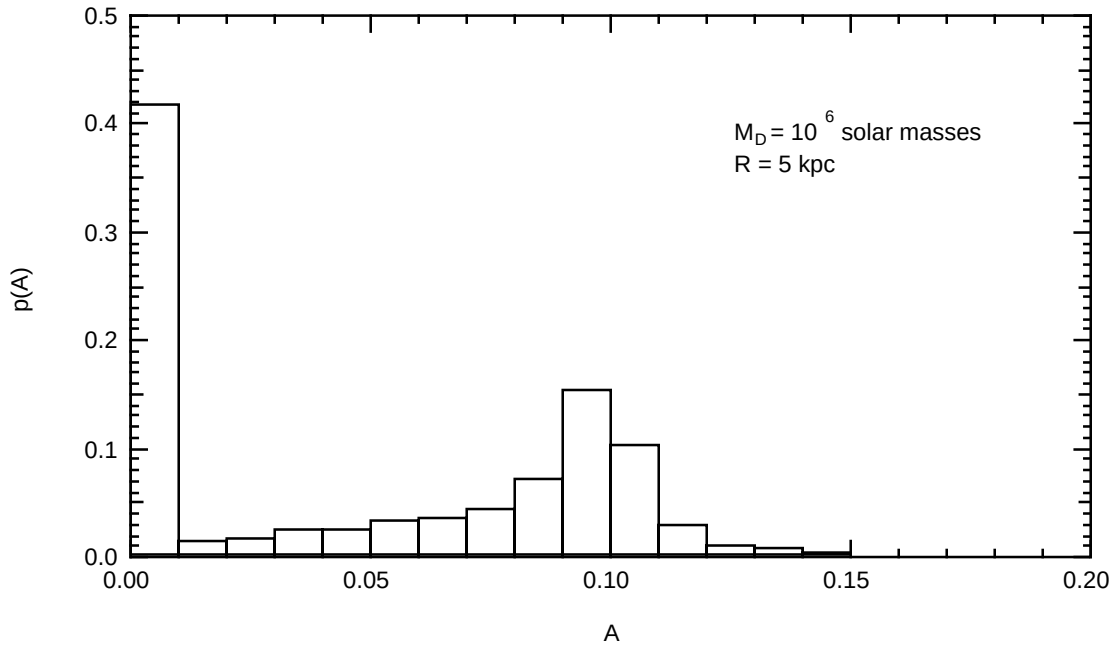

Fig. 9. Histogram of the probability p(A) to find a supernova with extinction between A and A+.01, plotted versus A, for the spheroidal galaxy dust model described in the text.

4. Comparison with supernova observations

4.1 Low-z supernova data

Phillips et al (1999) determine E(B-V) for 62 low-z Sne Ia, of which 39 are in spirals and 23 in spheroidal galaxies. They calculate E(B-V) from a weighted mean of $E(B-V)_{Tail}$, $E(B-V)_{Max}$, and $0.8 \bullet E(V-I)_{Max}$, where the subscripts "Tail" and "Max" refer to epochs of each supernova light curve. Their final result for E(B-V) for each supernova (listed in col. 7 of their Table 2) also takes into account a Bayesian "prior", based on the extinction model of Hatano, Branch, and Deaton (1998), and used to eliminate the inconvenience of negative E(B-V) values. Since our goal is to compare observed E(B-V) with predictions of our extinction models, we have recalculated the E(B-V) values of Phillips without the Bayesian prior, to obtain the binning listed in Table 5.

Table 5. Binning of E(B-V) for 62 supernovae. Data from Phillips (1999).

E(B-V)	# of Sne (Spirals)	# of Sne (Spheroidals)
-.05-.05	11	12
.05-.15	16	7
.15-.25	6	1
.25 - ∞	6	3

The typical uncertainty for each E(B-V) in Table 5 is .03 to .05.

Comparison of the data of Table 5 with the predictions of our models is bound to be extremely crude, given the small numbers of events in Table 5 and the relatively large uncertainty in E(B-V) for each of them. Furthermore, several of the events in the bins .25-∞ for columns 2 and 3 of Table 5 are known to be in galaxies with unusual dust lanes. We proceed nevertheless by first considering the 36 of the 39 spirals for which cos θ values are known (Ivanov 2000). Here, the average value of cos θ is .54 (.04), and a histogram of the 36 values suggests a more-or-less uniform distribution of cos θ with some deficiency of Sne Ia for small cos θ (edge-on spirals.) Thus we make predictions from the spiral galaxy model for numbers of supernovae in the same bins as col. 2. of Table 5, assuming B/T=.15, cos θ uniformly and randomly distributed between 0 and 1, and no restriction on radial distance of the supernova from the galactic center. The value of E(B-V) is determined from A and an assumed value of R_V, according to the following formula derived from (6):

$$E(B-V) = A\left[\frac{.932 + .003R_V}{1.003R_V + .932}\right] \qquad (32)$$

The results are displayed in Fig. 9, where we plot χ^2 per degree of freedom for a fit of the model to the data as a function of b, with R_V=3.1. The figure suggests that for supernovae in spiral galaxies, values of b in the neighborhood of 0.3-0.4, rather than higher values of b, are favored. Although the minimum value of χ^2 is not impressive, this conclusion concerning b appears to be quite robust. In particular, it is insensitive to changes in B/T, and to rather large changes in R_V.

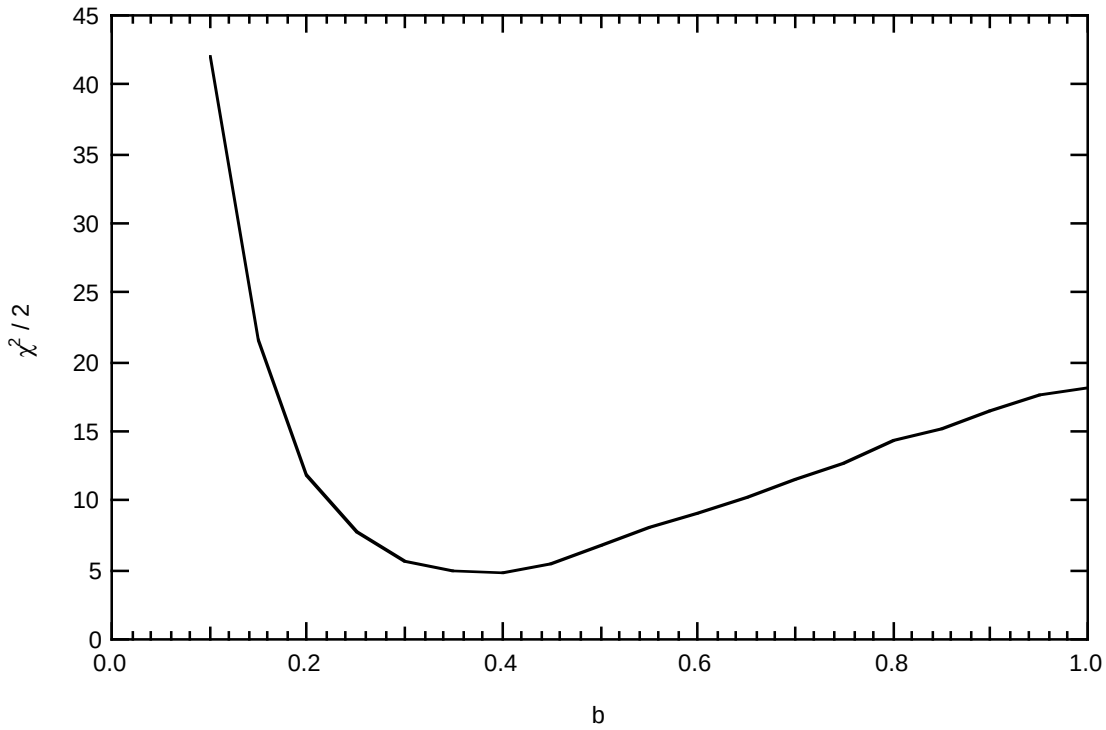

Fig.9. Comparison of E(B-V) binning for spirals in Table 5 with the predictions of the spiral galaxy model for the same bins. χ^2/dof = χ^2/2 is plotted versus b for R_V=3.1.

A similar analysis for the supernovae in spheroidal galaxies is even cruder, given the smaller number of events, 23, and the fact that at least one supernova (1986G) is in a very unusual host galaxy with peculiar dust lanes (NGC 5128). Proceeding nevertheless with our spheroidal model, we find a reasonably good fit to the values in the third column of Table 5 by assuming a dust mass of $\approx 2 \bullet 10^6$ solar masses, R_V in the range 2 to 3.1, and R ≈5 kpc. In view of the obvious uncertainties in the data and in the model assumptions, these results are reasonably consistent with the conclusions of Wise and Silva. On the other hand, the uncertainties are so large that we cannot place any strong constraints on the model.

4.2 High-z supernova data

As mentioned in Sec. 2, the morphological types of 39 high-z Sne Ia host galaxies have been classified by Sullivan and Ellis, [Sullivan 2002]. The E(B-V) values for 33 of these supernovae are known, and appear in Table 6. This table also contains a "critical extinction" A_{crit} for each of 26 supernovae, determined from conditions of observation, as well as the projected galactocentric radii of these supernovae (Aldering 2002). Note that of the 33 supernovae listed with E(B-V) values in Table 6, only 2 (1996cg and 1996 cn) have E(B-V) >0 with at least 95% confidence.

Although the individual E(B-V) uncertainties of the 33 supernovae are large, we attempt to interpret the results of Table 6 as follows. First we average the critical extinctions of the 26 supernovae for which the latter quantity is listed, and find $<A_{crit}>$=1.28±.13. Then we choose the upper limit of this quantity to serve as A_0 = 1.41, which corresponds to a limiting red-shift z_0=.90. Using our spiral galaxy model we

then calculate the average E(B-V) of all supernovae with extinctions less than or equal to A_0, as a function of b. In this calculation we choose cos θ random and uniform between 0 and 1, place no restriction on the projected radius, set R_V=3.1, and choose B/T=.15, or B/T=.40. (The results are virtually identical for the latter two choices).

Fig. 10 shows the result of this calculation for B/T=.15. The solid curve in Fig. 10 represents the calculated values of <E(B-V)> and the vertical lines within the graph indicate the dispersion of E(B-V) for b=.1,.2,… The three vertical lines (1), (2), (3) to the right of the graph indicate the weighted means and the uncertainties in these means for (1): the 17 late spirals of Table 6; (2): the 8 early spirals of Table 6, and (3): the same for the early and late spirals taken together. Obviously we have consistency between cases (1) or (3) and the model, but a mild inconsistency between case (2) and the model.

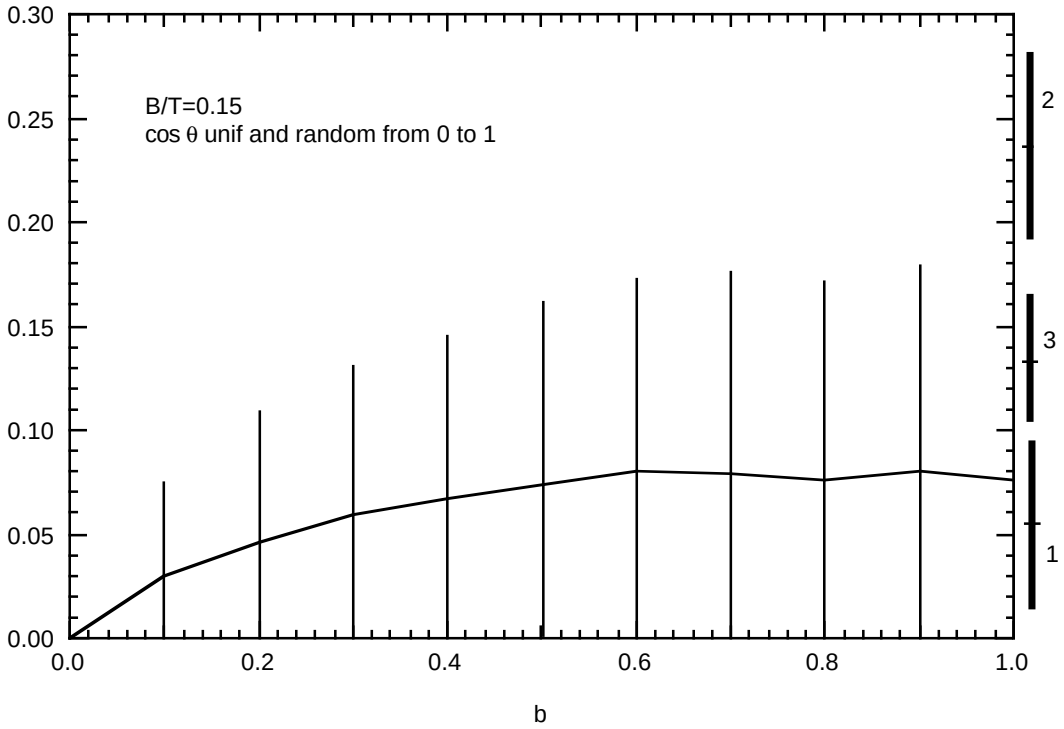

Fig.10 a): Average E(B-V) for all Sne with extinction less than or equal to 1.41, versus b for B/T=.15, cos θ uniform and random between 0 and1, and no restriction on projected galactocentric radius. Vertical lines inside graph indicate dispersion in calculated E(B-V). (1): Weighted mean and uncertainty in mean for late spirals; (2): Same for early spirals; (3): Same for early and late spirals taken together.

E(B-V) for each of the 8 spheroidal galaxies in Table 6 is consistent with zero, as is their weighted mean. In the spheroidal model, it turns out that any dust mass from 0 to $5 \cdot 10^6$ solar masses is consistent with these values; hence we can make no useful constraint on the dust mass.

5. Summary and Conclusions

We have constructed two simple host galaxy dust models, one for spiral galaxies and another for spheroidals, using well-known observational facts concerning dust, galaxy morphology, and star distributions as input. A number of simple conclusions concerning observational selection follow from the calculations, done particularly with the spiral galaxy model. In our view the most important of these is as follows: for uniform conditions of observation, a limiting red shift z_0 exists beyond which Sne Ia cannot be observed reliably. For any $z < z_0$ there is thus a limiting extinction $A_0(z)$ that decreases montonically as z approaches z_0. The average extinction <A> of all supernovae at z with extinction less than $A_0(z)$ also decreases montonically as z approaches z_0, and at any given z reaches a limiting value as b increases. It seems clear that this effect must have a significant impact on the interpretation of observations of many Sne Ia done under uniform conditions, such as would occur with the proposed space observatory SNAP.

Comparisons between observed supernova extinction (as manifested in E(B-V)) and the predictions of the models are given for low-z and high-z supernova data. The models and the data are for the most part consistent; however, the uncertainties in the observed values of E(B-V) are so large that critical tests of the models are not yet possible. We do find that for low-z supernovae in spirals, b values in the range 0.35 to 0.45 are favored. For high z, the late spiral data are also consistent with the model, but the early spiral data are not quite consistent with the model, chiefly because of just 2 supernovae with unusually large values of E(B-V).

It seems clear that more critical tests will be possible for low-z when data from the "Supernova factory" become available (Wood-Vasey 2001); for low and intermediate z when data is obtained from the Canada-France collaboration (ref), and in the high-z case if and when the space observatory SNAP becomes a reality.

Interesting and helpful discussions with G.Aldering, G. Blanc, S. Deustua, A. Howell, A. Kim, C. Pennypacker, S. Perlmutter, M. Sullivan, and R. Vogel are gratefully acknowledged.

Table 6. Type Ia Supernovae classified as to host galaxy type by Sullivan and Ellis (2002). Col.1: Sn name; col. 2: red-shift z; col.3: galaxy type: [0:spheroidal, 1: early spiral, 2: late spiral]; col 4: E(B-V); col 5: estimated critical extinction based on "seeing"; col(6): projected galactocentric radius of supernova as fraction of 90% isophote.

Name	z	Type	E(B-V)	Crit A	PR/90
1997ac	0.32		.01(.07)		0.07
1997ai	0.45		.33(.11)		
1997s	0.612		-.59(.42)	1.2	0.147
1994am	0.372	0			
1995ba	0.388	0	0.0(0.1)	1.5	0.093
1995aw	0.4	0	-.08(.13)	2	0.368
1994al	0.42	0			
1997q	0.43	0	.09(.14)	0.5	0.018
1997h	0.526	0	.16(.18)	1.2	0.048
1995ax	0.615	0	-.14(.26)	1.1	0.147
1997j	0.619	0	.13(.43)	1	0.083
1996ck	0.656	0	-.12(.64)		0.139
1996cl	0.828	0	-.13(.16)		
1994f	0.354	1			
1994h	0.374	1			
1996cn	0.43	1	.34(.09)	1.6	1.12
1995ar	0.465	1	.44(.32)	1	0.926
1997p	0.472	1	.19(.15)	1.7	0.463
1996cg	0.49	1	.30(.08)	1.5	0.728
1997f	0.58	1	.13(.19)	0.5	0.292
1997aj	0.581	1	-.07(.16)	3	0.668
1995at	0.655	1	.20(.11)	1.4	0.274
1997r	0.657	1	.09(.17)	1.1	0.195
1997i	0.172	2	.04(1.00)		
1997n	0.18	2	.09(1.00)		
1997o	0.374	2	.02(.17)	0.6	0.095
1994an	0.378	2			
1997am	0.416	2	.01(.11)	2.7	0.496
1994g	0.425	2	-.05(.21)	1.4	0.465
1995az	0.45	2	.07(.16)	0.6	0.953
1996cm	0.45	2	.14(.16)		0.261
1995aq	0.453	2	-.04(.16)	0.6	0.586
1992bi	0.458	2			
1995ay	0.48	2	.12(.17)	0.9	0.299
1996ci	0.495	2	.01(.09)	1.7	0.31
1995as	0.498	2	.11(.26)	0.7	0.468
1997l	0.55	2	-1.17(.92)	0.8	0.834
1996cf	0.57	2	.07(.09)		0.176
1997af	0.579	2	-.14(.23)	2.4	0.348
1997k	0.592	2	.22(.35)	0.7	0.369
1997g	0.763	2	-.44(.51)		
1997ap	0.83	2	.20(.11)		

References

Aguirre, A. (1999a) Ap. J. **512**, L19
Aguirre, A. (1999b) Ap. J. **525**, 583
Aguirre, A., and Haiman, Z.(2000) Ap. J. **532**, 28
Aldering, G. (2002). Private communication.
Annestad, P. A. and Purcell, E. M.(1973) ARAA **11**, 309
Bacon, R. (1960) J. Appl. Phys. **31**, 283
Balbi, A. et al (2000) Ap. J. **545**, L1
Binney, J. and Merrifield, M. (1998) *Galactic Astronomy* Princeton University Press, Princeton, New Jersey
Brinchmann, J. et. al. (1998) Ap. J. **545**, L1
Cardelli, J. A., Clayton, G. C., and Mathis, J. S. (1989) Ap J. **345**, 245
Carroll, S. M., Press, W. H., and Turner, E. L. (1992) ARAA **30**, 499
Davis, L. and Greenstein, J. L. (1951) Ap. J. **114**, 206
de Bernardis, P. et al (2000) Nature **404**, 955
de Vaucouleurs, G. (1948) Ann. Astrophys. **11**, 247
Donn, B., and Sears, G.W. (1963) Nature **140**, 1208
Draine, B. T., and Lee, H. M. (1984) Ap. J. **285**, 89
Falco, E.E. et al (1999) Ap. J. **523**, 617
Frank, F. C.(1949) Dis. Faraday Soc. **5**, 48,67
Fleming, T.A., Liebert, J. and Green, R.F. (1986) Ap.J. **308**, 176
Genzel, R., and Cesarsky, C. J. (2000) ARAA **38**, 761
Hall, J. S. (1949) Science **109**, 166
Hatano, K., Branch, D., and Deaton, J (1998) Ap. J. **502**, 177
Helfand, D. (2002) Private communication
Hillebrandt, W. and Niemeyer, J. C. (2000) ARAA **38**, 191 and refs therein
Hiltner, W. A. (1949) Science **109**, 165
Ishida, K. et al (1982) Pub. Ast. Soc. Japan **34**, 381
Ivanov, V. D., Hamuy, M., and Pinto, P.A. (2000) Ap. J. **542**, 588
Jaffe, A. H. et al (2001) Phys. Rev. Lett. **86**, 3475
Jansen, R.A. et al (1994) MNRAS **270**, 373
Keel, W.C. and White, R.E.(2001) A. J. **121**, 1442
Kent, S. M. (1985) Ap. J. Suppl. **59**,115
Knapen, J.H. et al (1991) AA **241**, 42
Linder, E. (2001) *Resource Book on Dark Energy*, Contributions from the Snowmass 2001 Workshop on the future of particle physics, ed. By E. Linder, Lawrence Berkeley National Laboratory, Berkeley, California
Mathews, L. D., and Wood, K. (2001) Ap J. **548**, 150
Mathis, J. S. (1990) ARAA **28**, 37
Mathis, J.S., Rumpl, W. and Nordsieck, K.H. (1977) Ap. J. **217**, 425
Mortsell, E., Gunnarsson, C., and Goobar, A.(2001) Ap.J. **561**, 106
Perlmutter, S. et al (1999) Ap. J. **517**, 517
Phillips, M.M. et al. (1999) A.J. **118**, 1766
Riess, A. G. et al (1998) A.J. **116**, 1009

Riess, A. G. et al (2001) Ap. J.**560**, 49
Roberts, M. S. and Haynes, M. P. (1994) ARAA **32**, 115
Salpeter, E. (1977) ARAA **15**, 267
Schlegel, D.J., Finkbeiner, D. P., and Davis, M. (1998) Ap. J. **500**, 525
Sears, G. W. (1955) J. Chem. Phys. **23**, 1630
Simien, F. and deVaucouleurs, G. (1986) Ap. J. **302**, 564
Soifer, B. T., Houck, J. R., and Neugebauer, G. (1987) ARAA **25**, 187
Sullivan, M. and Ellis, R.S. (2002) to be published
van den Bergh, S. and Tammann, G.A. (1991) ARAA **29**, 363
van den Bergh, S., Li, W, and Filippenko, A.(2002) to be published
Weingartner, J. C. and Draine, B. T. (2001) Ap. J. **548**, 296
Will, L. M., and Annestad, P. (1999) Ap. J. **526**, 242
Willson, L. A. (2000) ARAA **38**, 573
Wise, M. W. and Silva, D. R. (1996) Ap. J. **461**, 155
Wood-Vasey, W.M., et. al. (2001) Bull. A.A.S. **199**. 6408 W